Stratified turbulence at the buoyancy scale

Michael L. Waite[a)]
Department of Applied Mathematics, University of Waterloo, 200 University Avenue West, Waterloo, Ontario N2L 3G1, Canada

(Received 1 September 2010; accepted 14 May 2011; published online 23 June 2011)

Numerical simulations of forced stratified turbulence are presented, and the dependence on horizontal resolution and grid aspect ratio is investigated. Simulations are designed to model the small-scale end of the atmospheric mesoscale and oceanic submesoscale, for which high horizontal resolution is usually not feasible in large-scale geophysical fluid simulations. Coarse horizontal resolution, which necessitates the use of thin grid aspect ratio, yields a downscale stratified turbulence energy cascade in agreement with previous results. We show that with increasing horizontal resolution, a transition emerges at the buoyancy scale $2\pi U/N$, where U is the rms velocity and N is the Brunt–Väisälä frequency. Simulations with high horizontal resolution and isotropic grid spacing exhibit a spectral break at this scale, below which there is a net injection of kinetic energy by nonlinear interactions with the large-scale flow. We argue that these results are consistent with a direct transfer of energy to the buoyancy scale by Kelvin–Helmholtz instability of the large-scale vortices. These findings suggest the existence of a distinct subrange of stratified turbulence between the buoyancy and Ozmidov scales. This range must be at least partially resolved or parameterized to obtain robust simulations of larger-scale turbulence. © *2011 American Institute of Physics*. [doi:10.1063/1.3599699]

I. INTRODUCTION

Turbulence in fluids with strong stable density stratification is characterized by quasi-horizontal velocities and thin layers of strong vertical shear[1–4] (for a review of stratified turbulence, see Riley and Lelong[5]). The wide scale separation between the horizontal and vertical in such flows presents a difficulty for numerical simulation because it is costly to resolve the finely layered structure with isotropic grid spacing. This challenge is particularly serious in simulations of the atmosphere and ocean, where the typical vertical length scale may be orders of magnitude smaller than the horizontal. In such applications, the usual compromise is to employ grids with small aspect ratios, in which the vertical grid spacing Δz is much less than the horizontal spacing Δx. While such an approach may be appropriate for large-scale geophysical flows,[6] it cannot be expected to capture the transition to more isotropic three-dimensional turbulence at smaller scales. In this work, we investigate the nature of this transition, and its dependence on grid aspect ratio, in numerical simulations of homogeneous stratified turbulence.

There are two fundamental turbulent length scales associated with density stratification: the buoyancy scale

$$L_b \equiv 2\pi U/N, \tag{1}$$

where N is the Brunt–Väisälä frequency and U is the rms velocity, and the Ozmidov scale

$$L_O \equiv 2\pi\left(\epsilon/N^3\right)^{1/2}, \tag{2}$$

where ϵ is the total energy dissipation rate. The inclusion of the 2π factor in Eqs. (1) and (2) reflects the fact that it is often the corresponding wavenumbers k_b and k_O that emerge in applications. The buoyancy and Ozmidov scales have different dependence on N and reflect distinct physical processes. The buoyancy scale gives the thickness of the shear layers in stratified turbulence,[3,7] and is also associated with the zigzag instability of columnar vortices[8] and overturning of internal gravity waves.[9,10] By contrast, the Ozmidov scale is the outer scale of isotropic three-dimensional turbulence in stratified fluids.[11–13] Both L_b and L_O are much smaller than the energy-containing horizontal scale in stratified turbulence. Typical values in the atmosphere, assuming[14] $N = 0.01\ \mathrm{s}^{-1}$, $U = 10\ \mathrm{ms}^{-1}$, and $\epsilon = 10^{-4}\ \mathrm{m}^2\ \mathrm{s}^{-3}$, are $L_b \sim 6$ km and $L_O \sim 60$ m.

Lindborg[4] presented a theory and numerical evidence for an energy cascade from large to small horizontal scales in strongly stratified turbulence. From dimensional arguments, the horizontal and vertical wavenumber energy spectra associated with this cascade are predicted to be $E(k_h) \sim \epsilon^{2/3} k_h^{-5/3}$ and $E(k_z) \sim N^2 k_z^{-3}$, in agreement with previous predictions.[15,16] This theory assumes small horizontal Froude number, i.e., that the energy containing horizontal scale is much larger than both L_b and L_O. Although it has the same spectral slope, the stratified turbulence $-5/3$ spectrum is distinct from the isotropic three-dimensional Kolmogorov spectrum that is expected below the Ozmidov scale. Brethouwer *et al.*[17] have argued that a stratified turbulence inertial range extends from large scales down to the Ozmidov scale, where it transitions to isotropic three-dimensional turbulence, though this has not been demonstrated in simulations with a wide separation between L_b and L_O.

a)Electronic mail: mwaite@uwaterloo.ca.

Recent computational studies of turbulence in stratified fluids[2–4,17–19] have yielded horizontal spectra that are largely consistent with $k_h^{-5/3}$, while vertical spectral slopes are typically shallower than –3. However, stratified turbulence simulations are quite sensitive to how the buoyancy scale compares with the dissipation length scale L_d. Depending on the context, L_d may be the Kolmogorov viscous scale or, in numerical simulations with ad hoc diffusion, the scale of parameterized sub-grid scale turbulence. For the stratified turbulence cascade to be realized in numerical simulations, the dissipation scale must be much smaller than L_b.[3,4] When L_b and L_O are both inside the dissipation range, the turbulent cascade is suppressed by diffusive forces from vertical gradients, and a steep k_h^{-5} spectrum results.[3,17,18]

The computational challenge of stratified turbulence is that L_b and L_O are very small relative to the large energy-containing horizontal scales. It is simply impractical to perform simulations at geophysical Froude numbers with L_b and L_O well outside the dissipation range. Lindborg[4] proceeded by letting $\Delta z \ll \Delta x$ and using an anisotropic dissipation operator to keep the horizontal and vertical dissipation scales on the order of Δx and Δz, respectively. These simulations yielded an inertial range with $E(k_h) \sim \epsilon^{2/3} k_h^{-5/3}$ provided that L_b was resolved in the vertical (we use "resolved" in this paper to mean much larger than the dissipation scale). This agreement between theory and simulation gives support to the hypothesis that the cascade is driven by anisotropic eddies with horizontal scales much larger than L_b and thus suggests that fine horizontal resolution is not necessary.

Despite these successes, the use of grids that resolve L_b in the vertical but not the horizontal is potentially problematic because it effectively filters near-isotropic motions on small scales. There is a rich variety of motions at the buoyancy scale that are not represented correctly when $\Delta z \ll L_b \ll \Delta x$. These phenomena include Kelvin–Helmholtz instabilities,[18,20,21] overturning internal gravity waves,[9,10] saturating vortex instabilities,[22,23] and subsequent transition to isotropic three-dimensional turbulence.[9,11–13] All of these effects have the potential to interact with the downscale cascade of stratified turbulence, raising the possibility that a transition from stratified turbulence may occur at L_b rather than L_O. Indeed, bursts of shear instability have been found to excite intermittent peaks in the energy spectrum;[17,18] Laval *et al.*[18] suggested that the horizontal scale of these peaks corresponds to the typical vertical scale of the flow, which is presumably L_b.

The kinetic energy spectra in the atmospheric mesoscale[24–26] and oceanic submesoscale[27,28] are frequently observed to be close to $k_h^{-5/3}$ and k_z^{-3}. It has been proposed that a stratified turbulence cascade may be the basic mechanism behind these spectra.[4,29] At smaller scales, there have been some observations of transitions away from these spectral forms around the buoyancy scale, though the results are varied. In the free atmosphere, local maxima in kinetic energy at horizontal scales of around 1 km have been reported,[30] as have transitions to steep k_h^{-3} spectra at scales of 6 km.[31] By contrast, oceanic horizontal wavenumber spectra have been observed that exhibit a $k_h^{-5/3}$ range from hundreds of meters down to the Ozmidov scale.[28,32]

The question of buoyancy-scale motions and the extent that they need to be resolved in simulations of stratified turbulence are relevant for the accurate numerical modeling of the atmosphere and ocean. For the atmosphere, the connection between vertical resolution and energy spectrum is not as straightforward in realistic geophysical simulations as it is in idealized stratified turbulence experiments. A strong mesoscale cascade with an approximately $-5/3$ spectrum has been obtained in climate and weather prediction models with relatively coarse vertical resolution,[33–35] while high vertical resolution alone is not sufficient to guarantee a cascade.[36] A better understanding of the role of buoyancy scale dynamics in setting the kinetic energy spectrum and the consequences of not fully resolving them in the horizontal may help to clarify the relationship between stratified turbulence and simulations of the atmospheric mesoscale.

In this work, we use numerical experiments to explore how the energy cascade of stratified turbulence is affected by the resolution of small horizontal scales and how it ultimately transitions to a different turbulent regime. Our aims are threefold: to discover the scale at which this transition occurs; to understand the nonlinear transfers of energy across this scale; and to assess the ability of simulations with $\Delta z \ll \Delta x$ to capture the stratified turbulence cascade when this transition to small-scale turbulence is not resolved. The remainder of the paper is organized as follows. The numerical model and experimental set-up are outlined in Sec. II, and an overview of the simulations is given in Sec. III. In Sec. IV we analyze the sensitivity of the horizontal and vertical energy spectra to horizontal resolution, and discuss the transition in the spectrum that emerges at small scales when sufficient resolution is employed. In Sec. V we present the spectra of energy transfer and buoyancy flux, and diagnose the effects of nonlinear interactions between motions with large and small horizontal scales. Conclusions are given in Sec. VI.

II. APPROACH

A. Equations and numerical model

We employ the three-dimensional Boussinesq equations,

$$\frac{\partial \boldsymbol{u}}{\partial t} + \boldsymbol{u}\cdot\nabla\boldsymbol{u} = -\nabla p + b\hat{\boldsymbol{e}}_z + \boldsymbol{F} + D(\boldsymbol{u}), \tag{3}$$

$$\nabla\cdot\boldsymbol{u} = 0, \tag{4}$$

$$\frac{\partial b}{\partial t} + \boldsymbol{u}\cdot\nabla b + N^2 w = D(b), \tag{5}$$

where $\boldsymbol{u} = \hat{\boldsymbol{e}}_x u + \hat{\boldsymbol{e}}_y v + \hat{\boldsymbol{e}}_z w$ is the velocity, b is the buoyancy, p is the dynamic pressure divided by a reference density, $\boldsymbol{F}$ is the velocity forcing, and D is the dissipation operator. Coriolis forces are neglected. Constant N and triply-periodic boundary conditions are assumed, with domain size $L\times L\times H$. This configuration allows the use of a transform-based spectral method, which is integrated in time using the third-order Adams-Bashforth scheme. We use $n\times n\times m$ wavenumbers, yielding an effective grid resolution of $\Delta x \equiv \Delta y \equiv 1.5L/n$ and $\Delta z \equiv 1.5H/m$ after aliasing errors are eliminated with the 2/3 rule.[37] The spacing of

horizontal and vertical wavenumbers is $\Delta k_h \equiv 2\pi/L$ and $\Delta k_z \equiv 2\pi/H$.

At the length scales of interest in this work, direct numerical simulation (DNS) is not feasible and some model of sub-grid scale turbulence must be employed. Following a number of previous studies on geophysical turbulence,[3,4,19,38–40] we use a hyperviscosity/hyperdiffusion operator of the form

$$D \equiv (-1)^{p+1}(\nu_h \nabla_h^{2p} + \nu_z \partial_z^{2p}), \tag{6}$$

where p is a positive integer. Larger values of p yield shorter dissipation ranges, which is beneficial in problems that require a wide range of scales unaffected by dissipation. This scale selectivity is particularly necessary in the present work due to the wide separation of the forcing and buoyancy scales. Though ad hoc, hyperviscosity resembles other more sophisticated spectral-based large-eddy simulation approaches.[41]

We use $p=4$, for which the dissipation scale is[42]

$$L_d \equiv 2\pi\left(\nu_h^3/\epsilon\right)^{1/22}, \tag{7}$$

and the corresponding dissipation wavenumber is $k_d = 2\pi/L_d$. We refer to the two terms in Eq. (6) as horizontal and vertical diffusion, respectively. The coefficients ν_h and ν_z are chosen to be as small as possible while keeping the peak in the dissipation spectrum below the truncation wavenumber; in effect, we require $L_d \lesssim \Delta x$, as in DNS.[43] The same coefficients are used in the velocity and buoyancy equations. The horizontal and vertical coefficients are related by assuming that the grid-scale decay time is the same for both, i.e.,

$$\nu_z \equiv \nu_h(\Delta z/\Delta x)^8. \tag{8}$$

In addition to D, a weak linear damping is applied to modes with $k_h=0$ as a sink for the slow transfer of energy into them.[44]

B. Set-up of simulations

A summary of parameters and length scales for each simulation is given in Table I. The experiments are designed to be representative of the inner range of the atmospheric mesoscale and ocean submesoscale, with strong stratification, small aspect ratio, and no rotation (see Table II for representative parameter values and length scales in the atmospheric context). As in previous studies on stratified turbulence,[1,3,4] kinetic energy is injected by random forcing of barotropic vorticity with large-scale horizontal wavenumbers around $k_f \equiv 3\Delta k_h$. Low-level random noise is added to all fields at $t=0$ so that the ultimate forced-dissipative flow is fully three-dimensional despite the two-dimensional forcing.

The strength of the stratification of the large scales is characterized by the forcing-based Froude number[4]

$$Fr \equiv \epsilon^{1/3} k_f^{2/3}/N. \tag{9}$$

We consider three stratifications, with $Fr=0.05$, 0.02, and 0.01; these correspond to simulation sets A, B, and C in Table I. The energy dissipation rate ϵ is related to the forcing amplitude and is therefore similar in all simulations; the Froude number is varied by changing N.

TABLE I. Summary of parameters and scalar quantities for each simulation. The values of Fr, L_b, L_O, and L_d are based on time-averaged ϵ. In the run labels, A, B, C denote stratification; 1, 2, 3, etc. denote horizontal resolution; and v denotes high vertical resolution.

Run	Fr	n	M	H/L	$\Delta z/\Delta x$	$\Delta x/L_b$	$\Delta x/L_O$	$\Delta x/L_d$
A1	0.047	128	128	0.125	0.125	0.43	3.4	0.35
A2	0.047	256	128	0.125	0.25	0.21	1.7	0.35
A3	0.046	512	128	0.125	0.5	0.10	0.88	0.36
A4	0.046	1024	128	0.125	1	0.053	0.45	0.34
B1	0.024	128	128	0.0625	0.0625	0.87	9.7	0.35
B2	0.024	256	128	0.0625	0.125	0.43	4.9	0.37
B3	0.023	512	128	0.0625	0.25	0.21	2.5	0.37
B4	0.024	1024	128	0.0625	0.5	0.11	1.3	0.38
B5	0.025	2048	128	0.0625	1	0.048	0.56	0.37
B3v	0.023	512	256	0.0625	0.125	0.20	2.4	0.37
B4v	0.023	1024	256	0.0625	0.25	0.10	1.3	0.38
C1	0.012	128	128	0.03125	0.03125	1.7	28	0.35
C2	0.012	256	128	0.03125	0.0625	0.86	13	0.37
C3	0.011	512	128	0.03125	0.125	0.43	7.1	0.39
C4	0.011	1024	128	0.03125	0.25	0.21	3.7	0.39
C5	0.012	2048	128	0.03125	0.5	0.095	1.6	0.41

The vertical extent of the domain H is chosen to be approximately $4.5L_b$, which is large enough to capture the characteristic layers of stratified turbulence. Most simulations use $m=128$, yielding $L_b/\Delta z \approx 20$. The vertical grid spacing is larger for smaller N and smaller for larger N to ensure that L_b is equally well resolved in the vertical for each stratification, as in Lindborg.[4] Two additional simulations with $m=256$ are also presented to demonstrate convergence with Δz.

In the horizontal, simulations are performed with a wide range of Δx. The coarsest (with $n=128$) does not resolve the buoyancy scale, while the highest ($n=2048$) is fine enough to resolve L_b but not L_O. The highest resolution grids have aspect ratios of 1 or 1/2. For each stratification, simulations are spun up at the lowest resolution for 40 nonlinear timescales τ_N, where

$$\tau_N \equiv \epsilon^{-1/3} k_f^{-2/3}. \tag{10}$$

TABLE II. Dimensional parameter values and length scales for simulations with $Fr=0.02$ (runs B1-B5) in the atmospheric mesoscale context.

N	Brunt–Väisälä frequency	0.01 s^{-1}
L	Horizontal domain size	50 km
H	Vertical domain size	3.125 km
Δx	Horizontal grid spacing	580 m down to 36.6 m
Δz	Vertical grid spacing	36.6 m
ϵ	Energy dissipation rate	$\approx 10^{-4}$ m^2 s^{-3}
U	rms velocity	≈ 1 ms^{-1}
L_b	Buoyancy scale	≈700 m
L_O	Ozmidov scale	≈60 m
τ_N	Nonlinear timescale	≈1.2 h

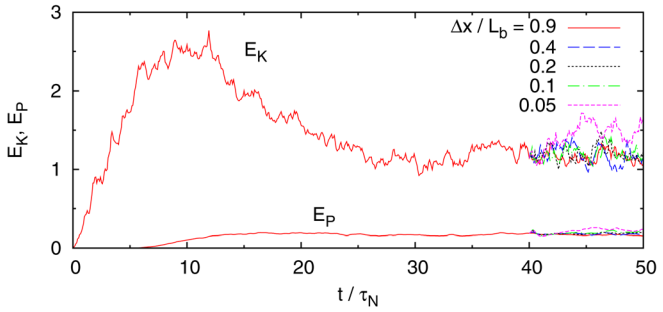

FIG. 1. (Color online) Time series of total kinetic energy E_K and potential energy E_P in simulations with $Fr = 0.02$. Simulations are spun up with $\Delta x/L_b = 0.9$ and then restarted at $t = 40\tau_N$ with different horizontal resolutions.

Simulations are then continued for another $10\tau_N$ for every Δx. Reported values of Fr, τ_N, L_b, L_O, and L_d are based on time averages of ϵ and kinetic energy over the last $8\tau_N$ of the restarted simulations.

III. OVERVIEW OF SIMULATIONS

Time series of kinetic and potential energy are plotted in Fig. 1 for $Fr = 0.02$. Kinetic energy increases in the low-resolution simulations for the first $10\tau_N$, during which time the flow is essentially two-dimensional. After this time, kinetic energy decreases, potential energy increases, and the flow transitions to a statistically stationary three-dimensional state. The launching of the higher-resolution simulations at $t = 40\tau_N$ is visible in Fig. 1. For our range of parameters, the Ozmidov scale is an order of magnitude smaller than the buoyancy scale, and the highest resolution simulations have $\Delta x \ll L_b$ and $\Delta x \sim L_O$. The vertical Froude number Fr_z, which is computed using the rms horizontal component of the vorticity $\boldsymbol{\omega} \equiv \boldsymbol{\nabla} \times \boldsymbol{u}$, is approximately 1 for all simulations, as expected[3,7] (not shown).

Figure 2 shows vertical slices of the y-component of vorticity from each simulation at $Fr = 0.02$. The physical structures in the simulation display a significant dependence on horizontal resolution. At the lowest resolution, the flow comprises thin, vertically laminar shear layers. As the horizontal resolution increases, structures with aspect ratios closer to unity begin to emerge. At intermediate resolutions, these structures resemble intermittent Kelvin–Helmholtz instabilities. The highest-resolution simulation exhibits a wide variety of structures: laminar shear layers, Kelvin–Helmholtz instabilities, and what appears to be patches of three-dimensional turbulence. Indeed, some of the structures in the highest-resolution simulation look remarkably isotropic, even at the scale of the shear-layer thickness. Regions of three-dimensional turbulence are also visible in horizontal slices of vertical vorticity (Fig. 3) at high resolution.

IV. ENERGY SPECTRA

A. Horizontal spectra

Horizontal wavenumber spectra of total energy are plotted in Fig. 4. These spectra are computed by summing the energy in each wave vector $\boldsymbol{k}$ over k_z and binning into k_h intervals of width Δk_h. For kinetic energy, the spectrum is

$$E_K(k_h) \equiv \sum_{k_h - \Delta k_h/2 \le k_h' < k_h + \Delta k_h/2} \frac{1}{2}|\hat{\boldsymbol{u}}(\boldsymbol{k}')|^2, \qquad (11)$$

for k_h corresponding to positive integer multiples of Δk_h. Here hat denotes Fourier coefficient and $k_h'^2 = k_x'^2 + k_y'^2$. The potential energy spectrum $E_P(k_h)$ is defined similarly, and $E(k_h) \equiv E_K(k_h) + E_P(k_h)$. All spectra are averaged in time over the last $8\tau_N$ of the simulations.

For $Fr = 0.02$ (Fig. 4(b)), the spectrum obtained with the coarsest horizontal resolution has a short power law range between the forcing and dissipation scales with a spectral slope of around –1.3 (here and below, slopes are measured by a least-squares power law fit between dimensionless wavenumbers 6 and 20). Though shallower than the theoretical value of $-5/3$, this slope is nevertheless consistent with previous findings at comparable Froude numbers.[4] The low-

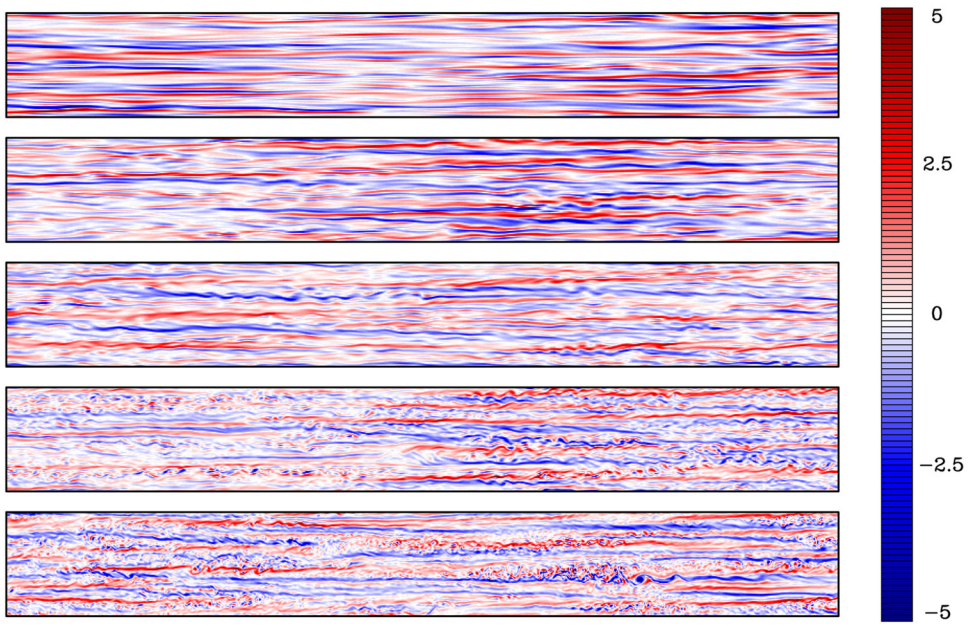

FIG. 2. (Color online) Vertical slices through the $y = 0$ plane of ω_y/N for $Fr = 0.02$ and (from top to bottom) $\Delta x/L_b = 0.9$, 0.4, 0.2, 0.1, and 0.05 (runs B1-B5 in Table I). For clarity, only half the domain $0 \le x \le L/2$ is shown. All fields are plotted at the end of the simulation.

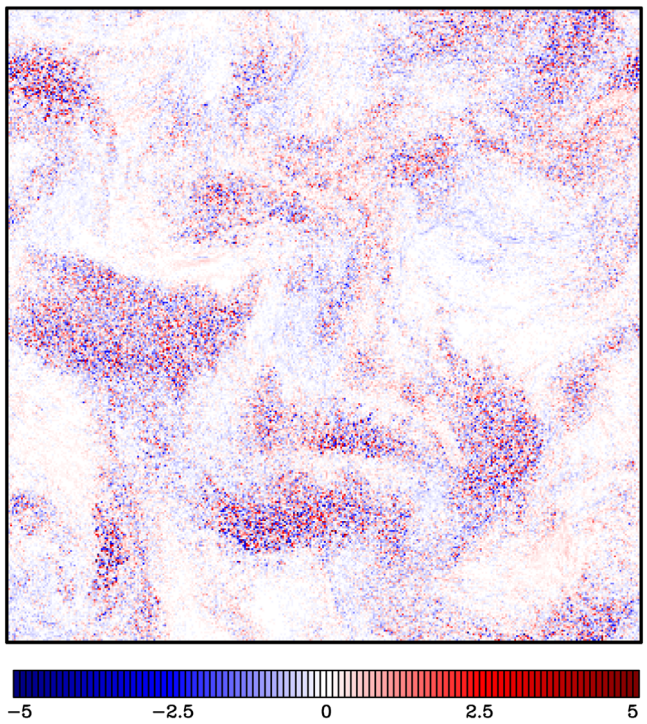

FIG. 3. (Color online) Horizontal slices through the $z=0$ plane of ω_z/N for $Fr=0.02$ and $\Delta x/L_b=0.05$ (run B5 in Table I) at the same time as in Fig. 2. Unlike in Fig. 2, the entire domain is shown.

resolution spectra at $Fr=0.05$ and 0.01 are similar. Note that the buoyancy wavenumber, marked (along with k_O) by arrows in Fig. 4, is not resolved in the horizontal by the lowest-resolution simulations at any stratification.

As the horizontal resolution is increased, the hyperviscosity coefficient ν_h is reduced and the k_h spectra extend to higher wavenumbers. The spectra vary in two nontrivial ways as Δx decreases towards Δz. First, the power law range gets steeper as finer horizontal scales are resolved, and at the highest resolution is noticeably steeper than $k_h^{-5/3}$. For $Fr=0.02$, the measured slopes are –1.6, –1.9, –2.0, and –2.1 for $\Delta x/L_b=0.4$, 0.2, 0.1, and 0.05. For $Fr=0.01$, the highest-resolution simulation has a slope of –2.2.

In addition to steepening, a transition in the k_h spectrum emerges as the horizontal resolution increases. At intermediate resolutions (e.g., $\Delta x/L_b=0.4$ and 0.2 for $Fr=0.2$) there is a shallow tail in the spectrum. The position of this tail appears to scale with k_d, implying that it is likely an artifact of the small-scale dissipation, possibly due to the bottleneck effect.[45] However, at the highest resolutions ($\Delta x/L_b=0.1$ and 0.05 for $Fr=0.2$) the location of the spectral transition appears to be independent of k_d; this robustness strongly suggests that the spectral transition in the high-resolution simulations is a real feature of the flow. In these high-resolution simulations, the energy spectrum has two distinct ranges between the forcing and dissipation scales: a large-scale power law range with a slope of around –2 and a small-scale bump. The position of the bump appears to be given by k_b, which can be seen by comparing the spectra at different resolutions and stratifications with the arrows in Fig. 4 (see also Fig. 10 below). We refer to the portions of the spectrum upscale and downscale of k_b as the mesoscale and microscale

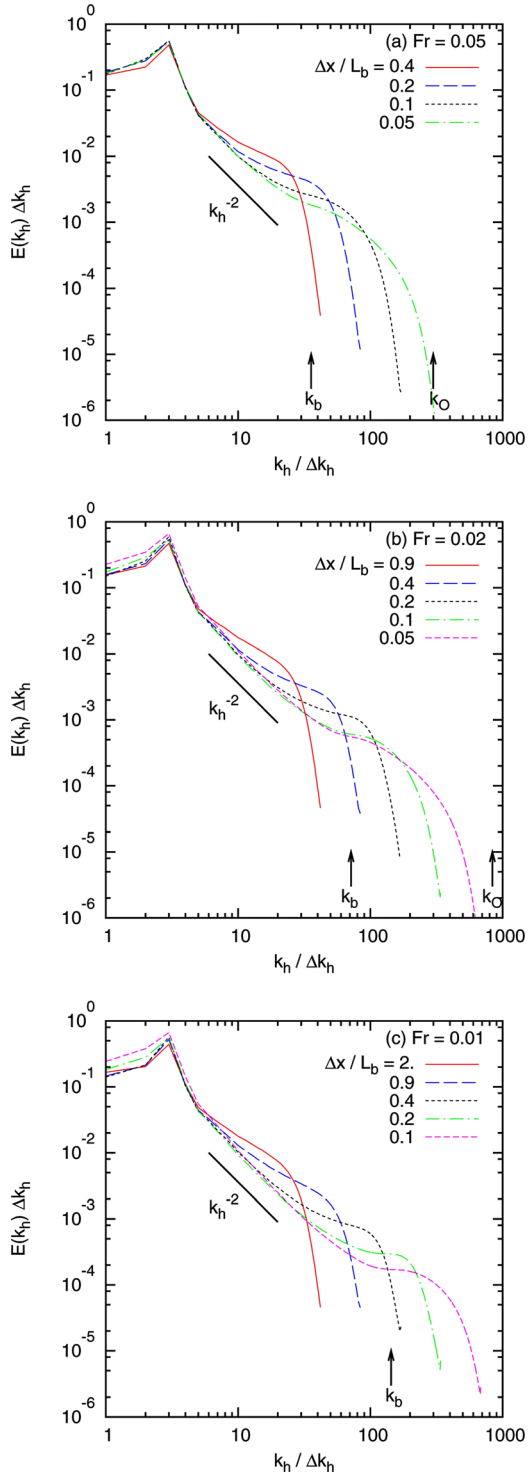

FIG. 4. (Color online) Horizontal wavenumber spectra of total energy for (a) $Fr=0.05$, (b) 0.02, and (c) 0.01. Dash patterns correspond to horizontal resolutions as indicated, and arrows mark the mean values of k_b and k_O.

ranges, respectively, based on the corresponding ranges in the atmosphere. Simulation B5 has the widest microscale range, with $k_d/k_b=8$.

Figure 5 compares the energy spectra from simulations with $Fr=0.02$ to corresponding runs with double the vertical resolution. Two cases are considered: $\Delta x/L_b=0.2$, in which the microscale transition is misrepresented as a shallow tail, and $\Delta x/L_b=0.1$, which gives a reasonably well-resolved transition. In both cases, the sensitivity of the spectra to

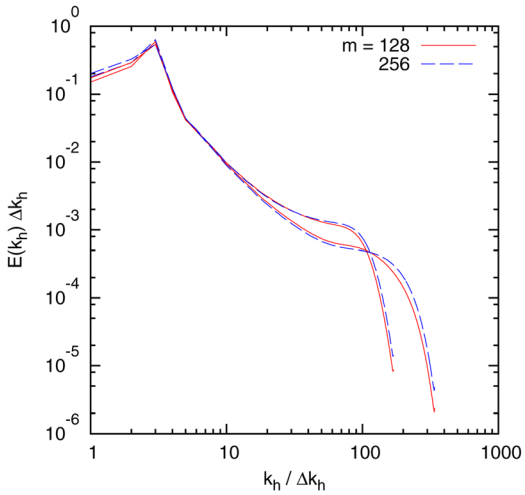

FIG. 5. (Color online) Horizontal wavenumber spectra of total energy for $Fr = 0.02$ with $\Delta x/L_b = 0.2$ and 0.1. Two vertical resolutions are shown: the standard value $m = 128$ (runs B3 and B4 in Table I; solid) and double resolution $m = 256$ (runs B3v and B4v in Table I; dashed).

decreasing Δz is negligible, indicating that the transition at k_b is not an artifact of insufficient vertical resolution.

Figure 6 shows the decomposition of the total energy spectra into kinetic, potential, vortex, and wave energy for the highest-resolution simulation with $Fr = 0.02$. Vortex and wave energies are computed using the linear normal mode basis,[46] in which vortex energy is the horizontally rotational kinetic energy, while wave energy is the sum of the divergent kinetic energy and potential energy. Kinetic and potential energy have the same mesoscale spectral slope, with the amplitude of the kinetic energy spectrum is equal to twice that of the potential. In the microscale range, the ratio of kinetic to potential energy is somewhat higher. The contribution to the kinetic energy from vertical motion (also plotted in Fig. 6(a)) is negligible at all scales. Interestingly, the vertical kinetic energy spectrum is approximately flat in the mesoscale range and has a local minimum at k_b. Apart from the largest scales, the total energy spectrum is dominated by wave energy. The mesoscale spectrum of vortex energy is significantly steeper than the wave spectrum, with a spectral slope of around –2.5.

Lindborg's[4] model kinetic energy spectrum $E_K(k_h) = 0.5\epsilon_K^{2/3} k_h^{-5/3}$, where ϵ_K is the kinetic energy dissipation rate, is plotted for reference in Fig. 6(a). The amplitude of this spectrum is in good agreement with our findings in the mesoscale range, though, as noted above, our spectrum is somewhat steeper. In the microscale range, by contrast, the Lindborg spectrum significantly underestimates the amount of kinetic energy.

B. Vertical spectra

Vertical wavenumber spectra of total energy are plotted in Fig. 7. These spectra are computed by summing over all k_x and k_y at each $|k_z|$, i.e., for kinetic energy

$$E_K(k_z) \equiv \sum_{k_z - \Delta k_z/2 \le |k'_z| < k_z + \Delta k_z/2} \frac{1}{2} |\hat{\boldsymbol{u}}(\boldsymbol{k}')|^2. \qquad (12)$$

All of the vertical spectra are characterized by a transition near k_b, in good agreement with the prediction that L_b is the

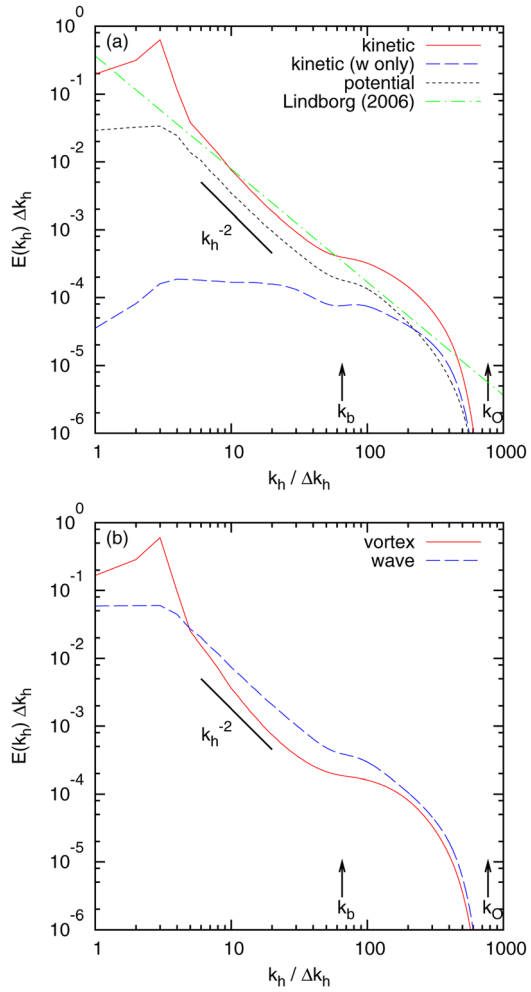

FIG. 6. (Color online) Horizontal wavenumber spectra of (a) kinetic, vertical kinetic, and potential energy, and (b) vortex and wave energy, for the highest-resolution simulation with $Fr = 0.02$ (run B5 in Table I). The Lindborg[4] kinetic energy spectrum is also shown, along with a reference line with a slope of –2.

dominant vertical scale in stratified turbulence.[3,7] As found by Waite and Bartello,[3] the spectrum is relatively flat upscale of k_b and falls off rapidly downscale. There is an approximate power law range downscale of k_b, the slope of which converges as the horizontal resolution increases. As more microscale turbulence is represented in the horizontal, the full range of k_z is affected; this dependence is to be expected since most of the k_z spectrum lies in the microscale. The highest resolution simulations have k_z spectral slopes of –2.5, –2.6, and –2.7 for $Fr = 0.05$, 0.02, and 0.01. These spectra are all shallower than k_z^{-3}, though they may be approaching this form as Fr decreases.

Figure 8 shows the vertical wavenumber spectra of kinetic, potential, vortex, and wave energy, again for the highest resolution simulation with $Fr = 0.02$. Downscale of k_b, the energy spectrum is dominated by kinetic over potential and wave over vortex energy. As was the case for the horizontal spectra, the amplitude of the kinetic energy spectrum is twice that of the potential energy, while their slopes are approximately equal. The kinetic energy spectrum is shallower and lower-amplitude than the predicted $N^2 k_z^{-3}$, which is included for reference in Fig. 8.

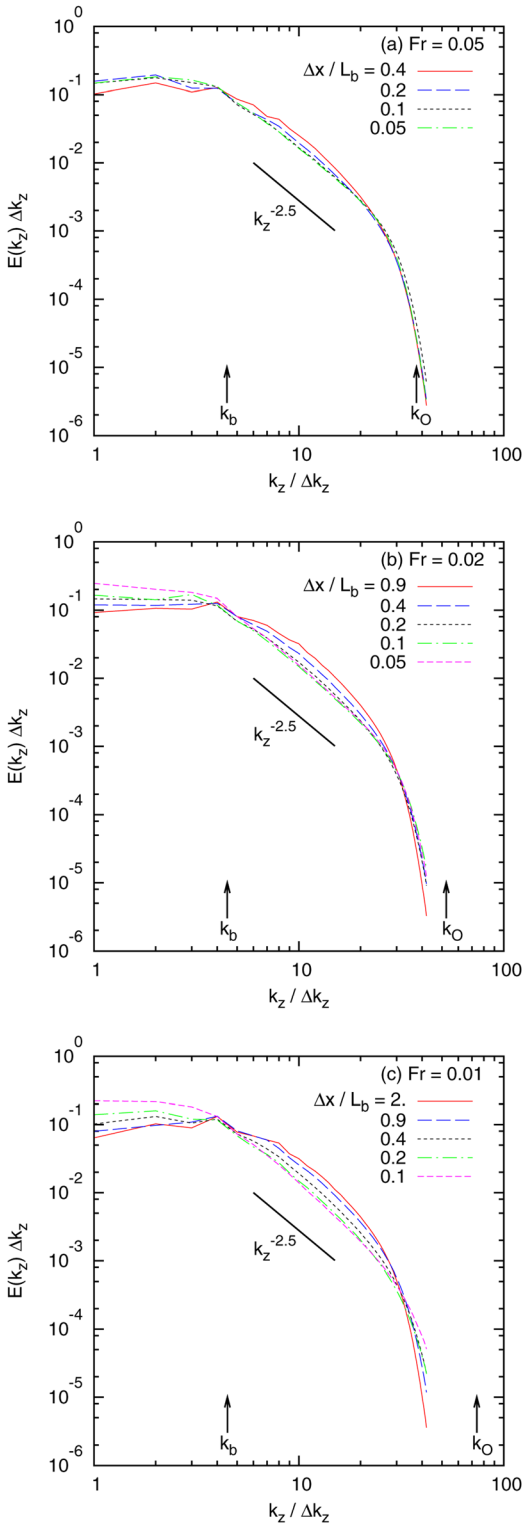

FIG. 7. (Color online) Vertical wavenumber spectra of total energy for (a) $Fr = 0.05$, (b) 0.02, and (c) 0.01. Dash patterns correspond to horizontal resolutions as indicated, and arrows mark the mean values of k_b and k_O.

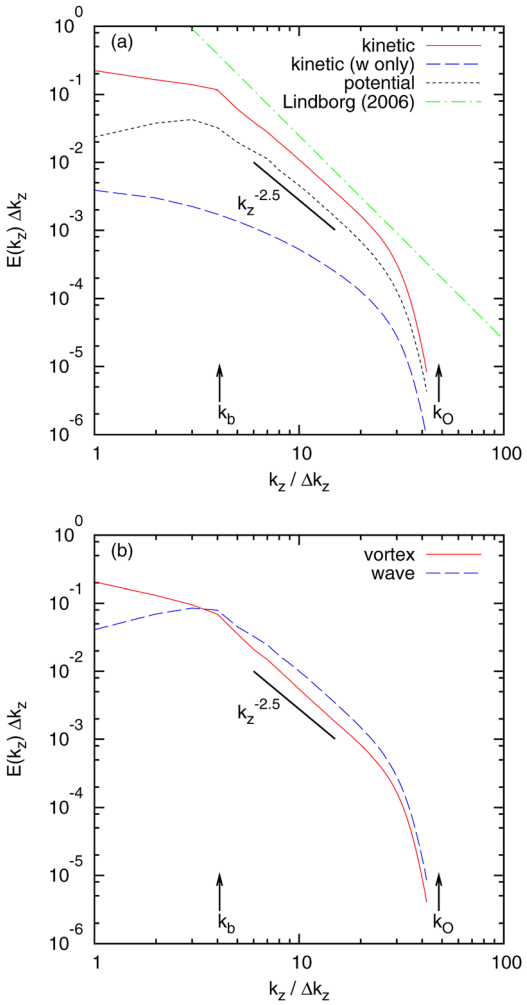

FIG. 8. (Color online) Vertical wavenumber spectra of (a) kinetic, vertical kinetic, and potential energy, and (b) vortex and wave energy, for the highest-resolution simulation with $Fr = 0.02$ (run B5 in Table I). The Lindborg[4] kinetic energy spectrum is also shown, along with a reference line with a slope of –2.5.

V. TRANSFER AND BUOYANCY FLUX SPECTRA

A. Global energy budget

The time evolution of the horizontal spectra of kinetic and potential energy is given by

$$\frac{\partial}{\partial t}E_K(k_h) = T_K(k_h) + B(k_h) - D_K(k_h) - \nu_h k_h^8 E_K(k_h) + F(k_h), \quad (13)$$

$$\frac{\partial}{\partial t}E_P(k_h) = T_P(k_h) - B(k_h) - D_P(k_h) - \nu_h k_h^8 E_P(k_h), \quad (14)$$

where $T_K(k_h)$ and $T_P(k_h)$ are the nonlinear transfer spectra of kinetic and potential energy, $B(k_h)$ is the buoyancy flux cross spectrum, and $F(k_h)$ is the forcing spectrum. Since these are horizontal wavenumber spectra, we consider the horizontal and vertical diffusion terms separately. The terms proportional to $\nu_h k_h^8$ in Eqs. (13) and (14) are the horizontal dissipation of kinetic and potential energy, which are (by design) non-negligible only in the horizontal dissipation range at large k_h. On the other hand, $D_K(k_h)$ and $D_P(k_h)$ are the horizontal spectra of vertical dissipation, which may have a different dependence on k_h.

The kinetic energy transfer spectrum $T_K(k_h)$ is the k_h spectrum (computed as in Eq. (11)) of the nonlinear term in the spectral kinetic energy equation

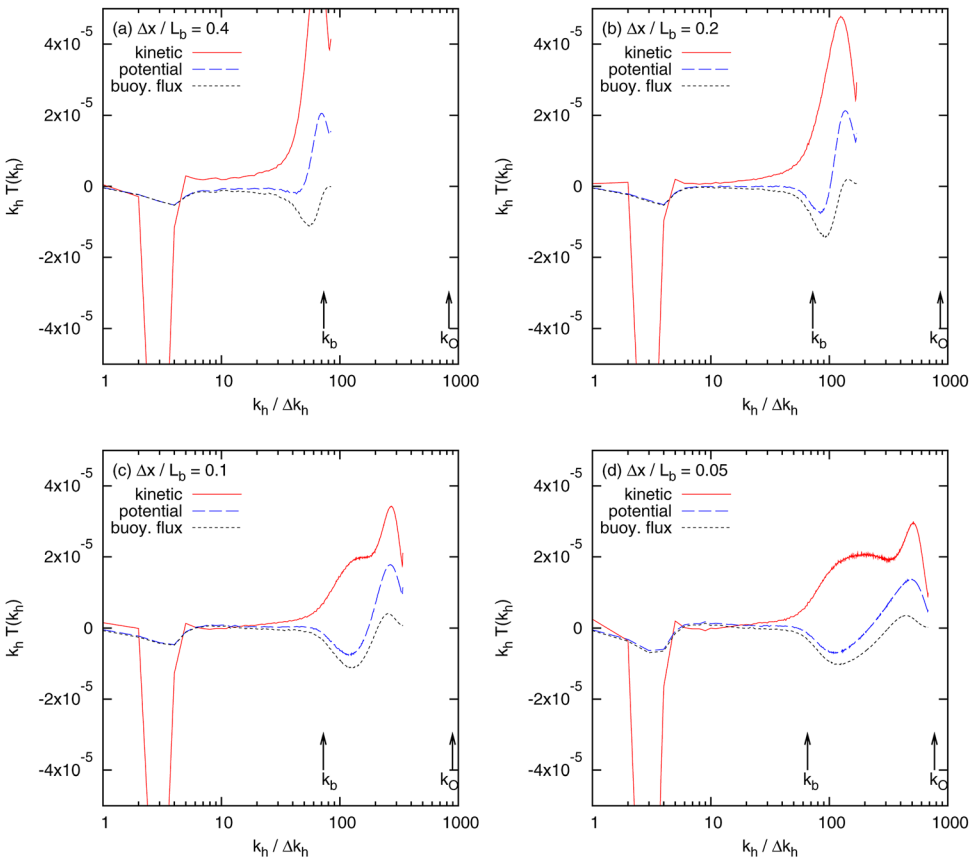

FIG. 9. (Color online) Horizontal wavenumber spectra of kinetic energy transfer, potential energy transfer, and buoyancy flux from simulations with $Fr = 0.02$ and $\Delta x/L_b =$ (a) 0.4, (b) 0.2, (c) 0.1, and (d) 0.05 (runs B2, B3, B4, and B5 in Table I). Note that the spectra are multiplied by k_h so that area is preserved with semilog coordinates.

$$T_K(\boldsymbol{k}) \equiv -\mathrm{Im} \sum_{\boldsymbol{k}+\boldsymbol{p}+\boldsymbol{q}=0} P_{ijm}(\boldsymbol{k})\hat{u}_j(\boldsymbol{p})\hat{u}_m(\boldsymbol{q})\hat{u}_i(\boldsymbol{k}), \qquad (15)$$

where P_{ijm} is the standard projection operator.[47] The $T_P(k_h)$ and $B(k_h)$ spectra are computed similarly.

For k_h between the forcing and horizontal dissipation ranges, the energy budget at statistical stationarity is a balance between two or three of the terms in Eqs. (13) and (14): nonlinear transfer, which transports kinetic and potential energy conservatively between different k_h; buoyancy flux, which converts kinetic energy to/from potential energy locally in k_h; and possibly vertical dissipation, which is not necessarily restricted to large k_h. Figure 9 shows the transfer and buoyancy flux spectra at four horizontal resolutions for $Fr = 0.02$. With a relatively coarse grid spacing of $\Delta x/L_b = 0.4$ (Fig. 9(a)), the mesoscale range is characterized by small positive $T_K(k_h)$ and negligible $T_P(k_h)$ and $B(k_h)$. The positive transfer of kinetic energy in the mesoscale is balanced by vertical dissipation, which is weak but non-negligible in this simulation. At large k_h the energy budget is dominated by peaks in the transfer spectra, which are balanced by the horizontal dissipation. These peaks are typical of a well-resolved dissipation range,[3,46,48] and are present in all of our simulations. Furthermore, they are consistent with the drop of the spectral energy flux to zero over the dissipation range.[4] There is also a negative buoyancy flux—i.e., conversion of kinetic to potential energy—at large k_h, suggesting that the turbulent fluxes in this regime lead to an excess of kinetic energy at the smallest horizontal scales. The energy balance in the lowest resolution simulation ($\Delta x/L_b = 0.9$, not shown) is similar.

With finer horizontal resolution, the mesoscale plateau of positive kinetic energy transfer is reduced (Figs. 9(b)–(d)). Energy transfer and buoyancy flux in this range are all small, implying independent cascades of kinetic and potential energy from k_h to k_b with little net exchange between them. However, a transition emerges around k_b in the two highest-resolution simulations (Figs. 9(c) and 9(d)). There is

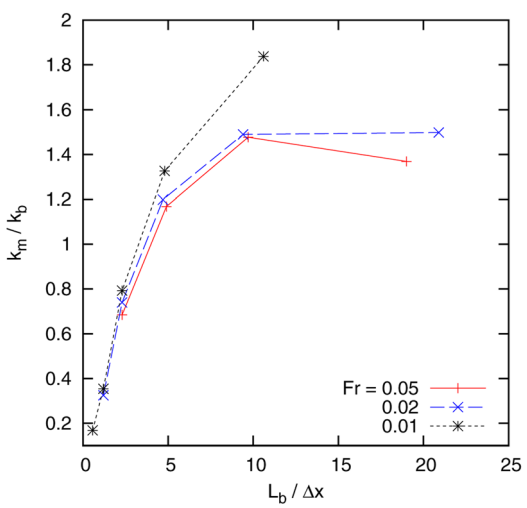

FIG. 10. (Color online) Horizontal wavenumber k_m of minimum small-scale buoyancy flux, scaled by k_b and plotted against $L_b/\Delta x$ for each simulation. Dash patterns denote stratification.

a significant positive peak in the kinetic energy transfer spectrum downscale of k_b, indicating an injection of kinetic energy into the microscale range. Some of this energy is converted to potential energy, as indicated by the negative peak in buoyancy flux. The rest is removed by vertical dissipation, which is not necessarily restricted to large k_h. The shape of the transfer and buoyancy flux spectra around k_b is relatively insensitive to a doubling of horizontal resolution from $\Delta x/L_b = 0.1$ to 0.05, which strongly suggests that the injection of kinetic energy here is not an artifact of the dissipation range but is rather a well-resolved physical phenomenon. Interestingly, there is positive buoyancy flux—i.e., conversion from potential to kinetic energy—at very large k_h. Similar small-scale restratification has been observed in previous simulations of stratified turbulence generated by breaking gravity waves.[9,48,49]

The length scale of kinetic energy injection into the microscale can be characterized by the horizontal wavenumber of minimum buoyancy flux at small scales, which we denote by k_m. Figure 9 suggests that this scale is proportional to the horizontal dissipation scale at low resolution and the buoyancy scale at high resolution, and this hypothesis is supported by our simulations at different stratifications. Figure 10 shows k_m/k_b for all experiments; it is plotted against $L_b/\Delta x$, which measures the degree to which the buoyancy scale is resolved in the horizontal. At low resolution of L_b, this quantity is approximately linear, indicating that $k_m \propto 1/\Delta x$. In this regime, the small-scale negative buoyancy flux is due to the effects of horizontal dissipation. As horizontal resolution of the buoyancy scale increases, the dependence of k_m/k_b on resolutions weakens. For high resolution, Fig. 10 suggests that k_m/k_b may approach a constant value. The curves for $Fr = 0.05$ and 0.02 show that $k_m \approx 1.5k_b$ for $L_b/\Delta x \approx 20$. With $Fr = 0.01$, for which we attain lower horizontal resolution of L_b, the value of k_b/k_b has not yet converged. Higher resolution simulations are necessary to confirm the asymptotic behavior of k_m/k_b for $\Delta x/L_b \to 0$. Nevertheless, these results strongly suggest that, as long as the microscale range of stratified turbulence is sufficiently resolved in the horizontal, there is a significant transfer of kinetic energy into scales of around L_b.

B. Mesoscale–microscale interactions

Interactions between mesoscale and microscale motions can be quantified by separating the sum over triads in Eq. (15) into large- and small-scale contributions, as is often done when diagnosing effective sub-grid scale dissipation.[50] This separation leads to a natural definition for the mesoscale energy transfer, in which $p_h, q_h \le k_b$ in Eq. (15); and microscale transfer, for which $p_h > k_b$ and/or $q_h > k_b$. The resulting mesoscale and microscale transfer spectra are shown in Fig. 11 for the highest-resolution simulations at $Fr = 0.02$ and 0.01. For clarity, only the mesoscale portion of the spectra ($k_h \lesssim k_b$) are shown.

Fig. 11 shows that while the transfer out of the large-scale forcing range is predominantly due to interactions with other mesoscale wavenumbers a nonnegligible amount is due to interactions with the microscale. In both cases shown

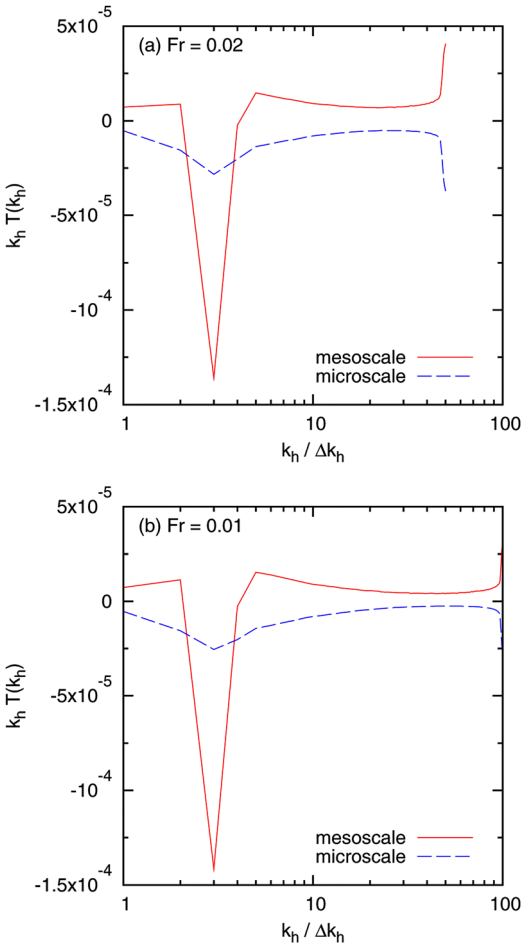

FIG. 11. (Color online) Mesoscale and microscale transfer spectra of total energy for the highest resolution simulations at (a) $Fr = 0.02$ and (b) 0.01 (runs B5 and C5 in Table I). For the purposes of separating the sum over triads into mesoscale and microscale interactions, the mesoscale–microscale transition is defined to be $k_h/\Delta k_h = 50$ for $Fr = 0.02$ and 100 for $Fr = 0.01$; actual values are 65 and 130, respectively. For clarity, only the mesoscale portion of the spectra is shown.

in Fig. 11, microscale interactions correspond to approximately 15% of the total transfer out of $k_h \approx k_f$. In addition, microscale interactions act as a drain on the energy throughout the mesoscale inertial range. The magnitude of this leakage from the inertial range appears to decrease as the separation between k_f and k_b increases, suggesting that it may be less significant at stronger stratifications where there is a wider separation between k_f and k_b.

The microscale transfer in Fig. 11 represents a direct, non-local transfer of energy from the forcing scale into the microscale. The microscale transfer around the forcing scale involves triads

$$\boldsymbol{k} = \boldsymbol{p} + \boldsymbol{q}, \tag{16}$$

in Eq. (15) with $k_h \approx k_f$ and at least one of $\boldsymbol{p}$ and $\boldsymbol{q}$ in the microscale, i.e., with horizontal component greater than k_b. But if $k_b \gg k_f$, as it is in our simulations, then Eq. (16) requires that both $\boldsymbol{p}$ and $\boldsymbol{q}$ be in the microscale. Energy transferred out of k_b by such interactions must therefore be going into $\boldsymbol{p}$ or $\boldsymbol{q}$, implying that the transfer of energy must be directly from large to small scales.

VI. CONCLUSIONS

We have presented numerical experiments of forced stratified turbulence that explore the nature and significance of dynamics on the buoyancy scale. It has been recognized for some time that these motions must be resolved in the vertical to obtain a strong downscale energy cascade in numerical simulations of stratified turbulence.[3,4] Such vertical resolution is usually feasible since L_b is often the energy-containing vertical scale of turbulent flows in stratified fluids.[7] However, horizontal resolution of the buoyancy scale is more computationally demanding because of the wide separation between the horizontal integral scale and L_b. One possible compromise, which is commonly made in numerical simulations of atmospheric and oceanic flows, is to employ numerical grids with small aspect ratios that resolve L_b in the vertical but not the horizontal. In this work, we have analyzed simulations with a wide range of horizontal grids to investigate the dynamics that emerge when the buoyancy scale is resolved isotropically, and to diagnose the effect that these motions have on the larger scales.

We have demonstrated that stratified turbulence simulations are in fact quite sensitive to horizontal resolution of the buoyancy scale. When Δx is coarse and L_b is not resolved, we obtained horizontal wavenumber energy spectra somewhat shallower than $k_h^{-5/3}$ between the forcing and dissipation scales. As Δx is decreased below the buoyancy scale, a transition emerges in the energy spectrum around k_b. At scales below the buoyancy scale, i.e., the microscale, the energy spectrum shallows into a broad bulge. The energy budget in this range is distinct from the inertial range at larger horizontal scales and is characterized by a significant injection of kinetic energy from nonlinear interactions. The microscale bulge does not appear to be an artifact of the dissipation range: as long as high horizontal resolution $(\Delta x/L_b \lesssim 0.1)$ is employed, its position is relatively insensitive to the dissipation scale L_d.

There is a physical explanation for this buoyancy-scale transition in the energy spectrum that is largely consistent with the stratified turbulence phenomenology described by Lilly,[20] with the exception of his conjecture of an inverse energy cascade. In this description of stratified turbulence, strong stable stratification leads to a vertical decoupling of layerwise horizontal motions and a collapse of the characteristic vertical scale. Ultimately, as foreseen by Lilly,[20] the vertical scale decreases sufficiently to make the Richardson number $O(1)$, at which point the flow becomes subject to Kelvin–Helmholtz instability. For the largest-scale vortices, which have a velocity scale given by the rms velocity U, this critical vertical scale must be on the order of the buoyancy scale. Indeed, the physical-space structures in our highest-resolution simulations strongly suggest the presence of intermittent bursts of shear instabilities and the subsequent transitions of these instabilities to three-dimensional turbulence. It is reasonable to expect, as described by Laval *et al.*,[18] that such instabilities will manifest as bumps in the horizontal energy spectrum.

It is significant that the small-scale breakdown of the stratified turbulence cascade occurs at the buoyancy scale, i.e., a scale larger than the Ozmidov scale in these simulations. Both quantities give length scales at which the Froude number is $O(1)$; the difference is in the velocity used to construct the Froude number. The buoyancy scale employs the rms velocity U, corresponding to the large-scale vortices. By contrast, the Ozmidov scale uses a spectrally local velocity $(k_h E(k_h))^{1/2}$ along with a Kolmogorov[51] or Lindborg[4] energy spectrum. The emergence of a transition at L_b strongly suggests that a non-local interaction, possibly Kelvin–Helmholtz instability of the large-scale vortices, is responsible for the injection of energy into the microscale. The decomposition of the energy transfer spectra into large- and small-scale contributions is consistent with this picture. The implication is that there is a direct transfer of energy from the energy-containing scales to the buoyancy scale. Deloncle *et al.*[22] called this type of transfer a "shortcut" to dissipation, because it bypasses the turbulent cascade and provides a direct link between the largest scales and the buoyancy scale.

The buoyancy and Ozmidov scales have a different dependence on N, and the separation between them grows with increasing stratification. Assuming[4] the relation $\epsilon = U^3 k_f$, it can be shown that $L_O/L_b \sim Fr_f^{1/2}$. As a result, there may be three distinct spectral ranges in strongly stratified turbulence: the mesoscale range, given by horizontal scales larger than L_b; the microscale range, between L_b and L_O; and the Kolmogorov inertial range, corresponding to scales smaller than L_O. Since the length of the microscale range is $Fr_f^{1/2}$, it may be too short to observe at only moderately small Froude numbers, for which L_b and L_O are of the same order. Higher-resolution simulations are necessary to investigate how the microscale transitions to isotropic three-dimensional turbulence below k_O.

Our experiments also indicate that simulations of the mesoscale inertial range are sensitive to the resolution of buoyancy scale motions. As the horizontal grid scale is refined below L_b, the mesoscale energy spectrum steepens to k_h^{-2}, which is slightly different from the $-5/3$ spectrum proposed by Lindborg.[4] It may be that this difference results from finite Froude number and that the spectral slope will converge to $-5/3$ as the Froude number is decreased further. However, this possibility seems unlikely given that Lindborg's[4] intermediate Froude number spectra were shallower, not steeper, than $k_h^{-5/3}$. Indeed, spectral slopes of -2 have been found in other studies of stratified turbulence.[52] These results raise the possibility that ad hoc sub-grid scale parameterizations, such as Eddy viscosity and hyperviscosity, may yield a poor representation for the effects of unresolved microscale turbulence on the mesoscale.

This study provides an illustration of the importance of choosing a numerical truncation that is appropriate for the underlying physics. At first glance, the large-scale anisotropy of stratified turbulence suggest the use of a numerical grid with $\Delta z \ll L_b \ll \Delta x$. Such a truncation effectively filters all dynamics with horizontal scales on the buoyancy scale, and is therefore only appropriate if these dynamics are unimportant. We have shown that they are in fact important because of the direct transfer of energy into these scales. Spurious numerical results from imposed grid anisotropy have also been

found in other fluid dynamical contexts, such as thermal convection.[53] In real stratified fluids with a full spectrum of motions, it is likely that this nonlocal transfer to the microscale coexists with a cascade of stratified turbulence. Indeed, it is possible that Lindborg[4] obtained such clean $-5/3$ spectra because his truncation eliminated this competing mechanism, leaving only the downscale cascade to determine the form of the energy spectrum.

Finally, isotropic resolution of the buoyancy scale in simulations of geophysical turbulence is computationally demanding, and so approximations must be made. One approximation is the representation of sub-grid scale diffusion with hyperviscosity; as computational resources increase, the nature of the mesoscale-microscale transition should ultimately be investigated with DNS with a sufficiently wide separation between the buoyancy, Ozmidov, and Kolmogorov scales. Another significant approximation is the use of ad hoc forcing to represent the large-scale source of energy. In geophysical turbulence, the ultimate source of this energy is baroclinic instability at atmospheric synoptic scales and the oceanic mesoscale. In such flows, frontogenesis and frontal instabilities provide an alternate mechanism for energy transfer to small scales.[54] The question of how large scale dynamics, for which Coriolis effects cannot be neglected, interact with the microscale is an essential one that requires further study.

ACKNOWLEDGMENTS

This work benefited greatly from conversations with and comments by Peter Bartello, Paul Billant, Lydia Bourouiba, Erik Lindborg, Piotr Smolarkiewicz, and two anonymous referees. Financial support from the Natural Sciences and Engineering Research Council of Canada and the University of Waterloo is gratefully acknowledged. Numerical simulations were performed on the Shared Hierarchical Academic Research Computing Network (SHARCNET).

[1]J. R. Herring and O. Métais, "Numerical experiments in forced stably stratified turbulence," J. Fluid Mech. **202**, 97 (1989).
[2]J. J. Riley and S. M. de BruynKops, "Dynamics of turbulence strongly influenced by buoyancy," Phys. Fluids **15**, 2047 (2003).
[3]M. L. Waite and P. Bartello, "Stratified turbulence dominated by vortical motion," J. Fluid Mech. **517**, 281 (2004).
[4]E. Lindborg, "The energy cascade in a strongly stratified fluid," J. Fluid Mech. **550**, 207 (2006).
[5]J. J. Riley and M.-P. Lelong, "Fluid motions in the presence of strong stable stratification," Annu. Rev. Fluid Mech. **32**, 613 (2000).
[6]J. N. Reinaud, D. G. Dritschel, and C. K. Koudella, "The shape of vortices in quasi-geostrophic turbulence," J. Fluid Mech. **474**, 175 (2003).
[7]P. Billant and J.-M. Chomaz, "Self-similarity of strongly stratified inviscid flows," Phys. Fluids **13**, 1645 (2001).
[8]P. Billant and J.-M. Chomaz, "Theoretical analysis of the zigzag instability of a vertical columnar vortex pair in a strongly stratified fluid," J. Fluid Mech. **419**, 29 (2000).
[9]G. F. Carnevale, M. Briscolini, and P. Orlandi, "Buoyancy- to inertial-range transition in forced stratified turbulence," J. Fluid Mech. **427**, 205 (2001).
[10]M. L. Waite and P. Bartello, "Stratified turbulence generated by internal gravity waves," J. Fluid Mech. **546**, 313 (2006).
[11]J. L. Lumley, "The spectrum of nearly inertial turbulence in a stably stratified fluid," J. Atmos. Sci. **21**, 99 (1964).
[12]R. V. Ozmidov, "On the turbulent exchange in a stably stratified ocean," Izvestia Akad. Nauk. SSSR Atmos. Oceanic Phys. Ser. **1**, 853 (1965).
[13]A. E. Gargett, T. R. Osborn, and P. W. Nasmyth, "Local isotropy and the decay of turbulence in a stratified fluid," J. Fluid Mech. **144**, 231 (1984).
[14]J. Y. N. Cho and E. Lindborg, "Horizontal velocity structure functions in the upper troposphere and lower stratosphere. 1. Observations," J. Geophys. Res. **106**, 10223, doi:10.1029/2000JD900814 (2001).
[15]E. M. Dewan, "Stratospheric wave spectra resembling turbulence," Science **204**, 832 (1979).
[16]E. M. Dewan and R. E. Good, "Saturation and the "universal" spectrum for vertical profiles of horizontal scalar winds in the atmosphere," J. Geophys. Res. **91**, 2742, doi:10.1029/JD091iD02p02742 (1986).
[17]G. Brethouwer, P. Billant, E. Lindborg, and J.-M. Chomaz, "Scaling analysis and simulation of strongly stratified turbulent flows," J. Fluid Mech. **585**, 343 (2007).
[18]J.-P. Laval, J. C. McWilliams, and B. Dubrulle, "Forced stratified turbulence: Successive transitions with Reynolds number," Phys. Rev. E, **68**, 036308 (2003).
[19]Y. Kitamura and Y. Matsuda, "The k_h^{-3} and $k_h^{-5/3}$ and energy spectra in stratified turbulence," Geophys. Res. Lett. **33**, L05809, doi:10.1029/2005GL024996 (2006).
[20]D. K. Lilly, "Stratified turbulence and the mesoscale variability of the atmosphere," J. Atmos. Sci. **40**, 749 (1983).
[21]J. Werne and D. C. Fritts, "Stratified shear turbulence: Evolution and statistics," Geophys. Res. Lett. **26**, 439, doi:10.1029/1999GL900022 (1999).
[22]A. Deloncle, P. Billant, and J.-M. Chomaz, "Nonlinear evolution of the zigzag instability in stratified fluids: A shortcut on the route to dissipation," J. Fluid Mech. **599**, 229 (2008).
[23]M. L. Waite and P. K. Smolarkiewicz, "Instability and breakdown of a vertical vortex pair in a strongly stratified fluid," J. Fluid Mech. **606**, 239 (2008).
[24]G. D. Nastrom and K. S. Gage, "A climatology of atmospheric wavenumber spectra observed by commercial aircraft," J. Atmos. Sci. **42**, 950 (1985).
[25]G. D. Nastrom, T. E. VanZandt, and J. M. Warnock, "Vertical wavenumber spectra of wind and temperature from high-resolution balloon soundings over Illinois," J. Geophys. Res. **102**, 6685, doi:10.1029/96JD03784 (1997).
[26]J. Y. N. Cho, Y. Zhu, R. E. Newell, B. E. Anderson, J. D. Barrick, G. L. Gregory, G. W. Sachse, M. A. Carroll, and G. M. Albercook, "Horizontal wavenumber spectra of winds, temperature, and trace gases during the Pacific Exploratory Missions: 1. Climatology," J. Geophys. Res. **104**, 5697, doi:10.1029/98JD01825 (1999).
[27]A. E. Gargett, P. J. Hendricks, T. B. Sanford, T. R. Osborn, and A. J. Williams III, "A composite spectrum of vertical shear in the upper ocean," J. Phys. Oceanogr. **11**, 1258 (1981).
[28]J. M. Klymak and J. N. Moun, "Oceanic isopycnal slope spectra. Part II: Turbulence," J. Phys. Oceanogr. **37**, 1232 (2007).
[29]J. J. Riley and E. Lindborg, "Stratified turbulence: A possible interpretation of some geophysical turbulence measurements," J. Atmos. Sci. **65**, 2416 (2008).
[30]N. K. Vinnichenko, "The kinetic energy spectrum in the free atmosphere – 1 second to 5 years," Tellus **22**, 158 (1970).
[31]J. T. Bacmeister, S. Eckermann, P. A. Newman, L. Lait, K. R. Chan, M. Lowenstein, M. H. Proffitt, and B. L. Gary, "Stratospheric horizontal wavenumber spectra of winds, potential temperature, and atmospheric tracers observed by high-altitude aircraft," J. Geophys. Res. **101**, 9441, doi:10.1029/95JD03835 (1996).
[32]W. S. Holbrook and I. Fer, "Oceanic internal wave spectra inferred from seismic reflection transects," Geophys. Res. Lett. **32**, L15604, doi:10.1029/2005GL023733 (2005).
[33]J. N. Koshyk and K. Hamilton, "The horizontal kinetic energy spectrum and spectral budget simulated by a high-resolution troposphere-stratosphere-mesosphere GCM," J. Atmos. Sci. **58**, 329 (2001).
[34]W. C. Skamarock, "Evaluating mesoscale NWP models using kinetic energy spectra," Mon. Wea. Rev. **132**, 3019 (2004).
[35]K. Hamilton, Y. O. Takahashi, and W. Ohfuchi, "The mesoscale spectrum of atmospheric motions investigated in a very fine resolution global general circulation model," J. Geophys. Res. **113**, D18110, doi:10.1029/2008JD009785 (2008).
[36]M. L. Waite and C. Snyder, "The mesoscale kinetic energy spectrum of a baroclinic life cycle," J. Atmos. Sci. **66**, 883 (2009).
[37]D. R. Durran, *Numerical Methods for Wave Equations in Geophysical Fluid Dynamics* Springer, New York, 1999.
[38]P. Bartello, O. Métais, and M. Lesieur, "Coherent structures in rotating stratified turbulence," J. Fluid Mech. **273**, 1 (1994).

[39]K. B. Winters and E. A. D'Asaro, "Direct simulation of internal wave energy transfer," J. Phys. Oceanogr. **27**, 1937 (1997).
[40]J. Sukhatme and L. M. Smith, "Vortical and wave modes in 3D rotating stratified flows: Random large-scale forcing," Geophys. Astrophys. Fluid Dyn. **102**, 437 (2008).
[41]P. Bartello, O. Métais, and M. Lesieur, "Geostrophic versus wave eddy viscosities in atmospheric models," J. Atmos. Sci. **53**, 564 (1996).
[42]P. A. Davidson, *Turbulence* (Oxford University Press, Oxford, 2004).
[43]P. Moin and K. Mahesh, "Direct numerical simulation: A tool in turbulence research," Annu. Rev. Fluid Mech. **30**, 539 (1998).
[44]L. M. Smith and F. Waleffe, "Generation of slow large scales in forced rotating stratified turbulence," J. Fluid Mech. **451**, 145 (2002).
[45]A. G. Lamorgese, D. A. Caughey, and S. B. Pope, "Direct numerical simulation of homogeneous turbulence with hyperviscosity," Phys. Fluids **17**, 015106 (2005).
[46]P. Bartello, "Geostrophic adjustment and inverse cascades in rotating stratified turbulence," J. Atmos. Sci. **52**, 4410 (1995).
[47]H. A. Rose and P. L. Sulem, "Fully developed turbulence and statistical mechanics," J. Phys. **39**, 441 (1978).
[48]D. Ramsden and G. Holloway, "Energy transfers across an internal wave-vortical mode spectrum," J. Geophys. Res. **97**, 3659, doi:10.1029/91JC02819 (1992).
[49]P. Bouruet-Aubertot, J. Sommeria, and C. Staquet, "Stratified turbulence produced by internal wave breaking: Two-dimensional numerical experiments," Dyn. Atmos. Oceans **23**, 357 (1996).
[50]R. H. Kraichnan, "Eddy viscosity in two and three dimensions," J. Atmos. Sci. **33**, 1521 (1976).
[51]A. N. Kolmogorov, "The local structure of turbulence in incompressible viscous fluid for very large Reynolds number," Dok. Akad. Nauk. SSSR **30**, 301 (1941).
[52]Y. Kimura and J. R. Herring, "Diffusion in stably stratified turbulence," J. Fluid Mech. **328**, 253 (1996).
[53]Z. P. Piotrowski, P. K. Smolarkiewicz, S. P. Malinowski, and A. A. Wyszogrodzki, "On numerical realizability of thermal convection," J. Comput. Phys. **228**, 6268 (2009).
[54]M. J. Molemaker, J. C. McWilliams, and X. Capet, "Balanced and unbalanced routes to dissipation in an equilibrated Eady flow," J. Fluid Mech. **654**, 35 (2010).